In silico prediction and in vivo testing of promoters targeting GABAergic inhibitory neurons

Yosuke Niibori,[1] Robert Duba-Kiss,[2] Joseph T. Bruder,[3] Jared B. Smith,[3] and David R. Hampson[1,2]

[1]Department of Pharmaceutical Sciences, Leslie Dan Faculty of Pharmacy, University of Toronto, 144 College Street, Toronto, ON M5S 3M2, Canada; [2]Department of Pharmacology and Toxicology, Faculty of Medicine, University of Toronto, Toronto, ON M5S 3M2, Canada; [3]Research and Early Development, REGENXBIO, Inc., Rockville, MD, USA

Impairment of GABAergic inhibitory neuronal function is linked to epilepsy and other neurological and psychiatric disorders. Recombinant adeno-associated virus (rAAV)-based gene therapy targeting GABAergic neurons is a promising treatment for GABA-associated disorders. However, there is a need to develop rAAV-compatible gene-regulatory elements capable of selectively driving expression in GABAergic neurons throughout the brain. Here, we designed several novel GABAergic gene promoters. *In silico* analyses, including evolutionarily conserved DNA sequence alignments and transcription factor binding site searches among GABAergic neuronal genes, were carried out to reveal novel sequences for use as rAAV-compatible promoters. rAAVs (serotype 9) were injected into the CSF of neonatal mice and into the brain parenchyma of adult mice to assess promoter specificity. In mice injected neonatally, transgene expression was detected in multiple brain regions with very high neuronal specificity and moderate-to-high GABAergic neuronal selectivity. The GABA promoters differed greatly in their levels of expression and, in some brain regions, showed strikingly different patterns of GABAergic neuron transduction. This study is the first report of rAAV vectors that are functional in multiple brain regions using promoters designed by *in silico* analyses from multiple GABAergic genes. These novel GABA-targeting vectors may be useful tools to advance gene therapy for GABA-associated disorders.

INTRODUCTION

Impairment of GABAergic neurons causes epileptic, neurodevelopmental, and psychiatric disorders.[1–4] For example, Dravet syndrome is an intractable epilepsy disorder caused by mutations in neuronal sodium channel subunits that, in turn, induce global impairment of GABAergic neuronal activity.[1,5–7] One therapeutic strategy for Dravet syndrome, and other neurological disorders where GABAergic inhibition is impeded, is to enhance GABA neuronal activity in the brain. Recombinant adeno-associated virus (rAAV)-based gene therapy is a promising therapeutic approach for correcting deficiencies in GABAergic neurons. rAAV-compatible gene-regulatory elements that convey selective gene expression in GABAergic neurons in the central nervous system (CNS) have been derived from the *Dlx*,

Gad1, *Gad2*, and *Scn1a* genes.[8–12] These regulatory elements are capable of driving rAAV-mediated transgene expression in the general neuronal population, but differ in CNS distribution and GABAergic neuronal specificity. Transgene expression induced by *Dlx* enhancer elements, for example, is GABAergic neuron selective but restricted to the forebrain.[8] In contrast, a *Gad1* regulatory element showed wider transgene distribution, but lower GABAergic-selective expression than the *Dlx* elements.[10] *Gad2* and *Scn1a* regulatory elements show high GABAergic specificity and wider transgene distributions compared with the Dlx elements, but transgene expression is preferentially operative in the parvalbumin (PV)-expressing subset of GABAergic neurons.[11,12] Therefore, currently there are no rAAV-compatible gene-regulatory elements that mediate expression in all subtypes of GABAergic neurons across the CNS (see Duba-Kiss et al. for review).[13]

In this study, we report novel GABAergic-neuron-selective promoters for use in rAAV vectors. The properties of these rAAVs were assessed after injection into the cerebral spinal fluid (CSF) of newborn mice and after intrahippocampal and intracerebellar injections into adult mice. Our findings demonstrate the utility of advanced *in silico* promoter design and provide new tools for use in rAAV gene therapy. The GABA-targeting vectors studied here may be useful for developing gene therapies for treating GABA-related disorders such as epilepsy, autism, and schizophrenia.

RESULTS

In silico analyses of GABAergic gene-regulatory elements

To identify GABAergic neuronal promoters for rAAV9 vectors, we analyzed the 5′-upstream sequences of GABAergic neuronal genes by two different *in silico* strategies. Homology analysis was performed on the 5′-upstream sequence of the human and mouse *Gad1* genes using

a LAGAN pairwise genome alignment algorithm.[14] The analysis between human and mouse 5′-upstream sequences revealed four conserved DNA regions with more than 70% sequence identity within a 100-base window in the 4-kb upstream regions from the *Gad1* transcription start site (Figure 1A, red-colored regions). Figure S1 depicts the DNA sequences of the 5′ conserved regions and positions in the mouse *Gad1* gene. The homologous DNA regions between human and mouse genomes were also conserved, with similar sequence identity, in other mammalian genomes (chimpanzee, gibbon, crab-eating monkey, marmoset, pig, horse, dog, and cat). The conserved DNA regions in the mouse *Gad1* 5′-upstream sequence were ligated tandemly and used as a composite transcription regulatory element.

The homology analysis was followed by an examination of the transcription factor binding sites (TFBSs) in the 5′-upstream sequence of three GABAergic genes to identify GABAergic neuron-specific TFBSs: *Gad1* and *Gad2*, two isoforms of the GABA synthesis genes coding for glutamic acid decarboxylase 1 and 2, and *Slc32a1*, coding for Vgat, the vesicular GABA transporter. The TFBSs in the human and mouse 5′-upstream sequences of the GABAergic genes, *Gad1*, *Gad2*, and *Slc32a1*, were identified using the JASPAR transcription factor database.[15] The TFBS search revealed that 128 TFBSs were conserved in the human and mouse GABAergic genes (Figure 1B). The predicted TFBSs were likely to include TFBSs for GABAergic-neuron-specific regulation as well as for general neuronal transcription. To eliminate the TFBSs for general neuronal expression, we identified the TFBSs that are shared with the *Camk2a* gene expressed primarily in non-GABAergic glutamatergic excitatory neurons and removed them from the TFBSs identified from the GABAergic neuronal genes. This subtraction yielded 24 of the original 128 TFBSs, which were then classified as GABAergic regulatory element candidates (Figure 1C). Predictions of the binding sites of the 24 transcription factors revealed that 149 candidate sites (each with of length of 10–14 nucleotides) were present in a 17-kb segment of the mouse Gad1 gene 5′-upstream sequence from the start codon (Table S1). Those TFBS candidates were ligated into the vector in a concatenated fashion from the 5′ end to the 3′ end, thereby creating the 2,100-bp regulatory element used in the GABA-v4 promoter.

Design of GABA-targeting rAAV9 vectors

To evaluate the GABAergic neuronal specificity of the regulatory elements identified by *in silico* analysis, single-stranded rAAV9 vectors were synthesized for injection into mice. All rAAV9 constructs included a carboxy-terminal c-myc epitope tag fused to NaVβ1 (Figure 1D). The endogenous mouse NaVβ1 protein was used as the encoded transgene in this study. Although foreign fluorescent proteins are often used to analyze cell-type specificity and distribution of rAAVs, the expression of fluorescent proteins has been associated with an immune response and cell death.[16] In addition, there are no reports of human NaVβ1 gene (*SCN1B*) duplications, and we have not previously observed abnormal behaviors in mice after overexpression of NaVβ1.[10] Together, these observations suggest that the use of NaVβ1 is appropriate for the accurate assessment of promoter cell-type specificity and brain transgene distribution.
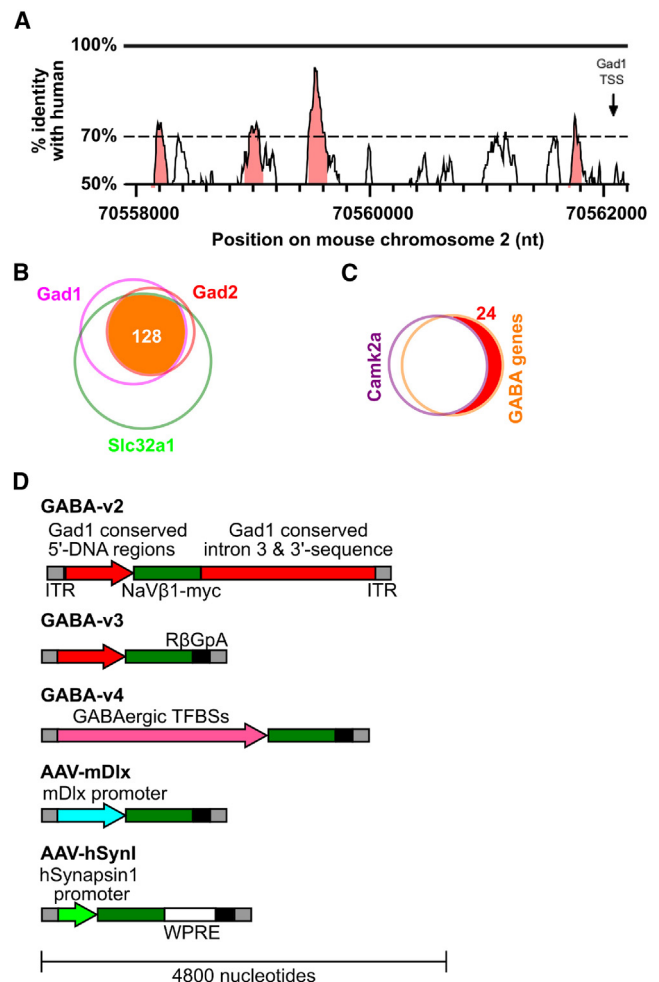

Figure 1. *In silico* analysis of GABA gene-regulatory elements

(A) Homology analysis of human and mouse *Gad1* gene sequences from the transcription start site (arrow) to 4 kb upstream in the 5′ untranslated region. The homology between *GAD1* on human chromosome 2 and *Gad1* on mouse chromosome 2 is depicted. The red-colored DNA regions indicate sections that are highly conserved between human and mouse. (B) Venn diagram of TFBSs conserved in the *Gad1*, *Gad2*, and *Slc32a1* 5′ intergenic sequences. One hundred twenty-eight TFBSs were identified (in orange) that overlap among *Gad1* (magenta), *Gad2* (red), and *Slc32a1* (green). (C) Selection of TFBSs for GABAergic genes. The TFBSs in *Camk2a*, a glutamatergic neuronal marker, were subtracted from the TFBSs of GABA genes, yielding 24 TFBSs as candidate GABA-selective elements. (D) DNA constructs of rAAV9 vectors. DNA components of GABA-v2 (GABA.v2-NaVβ1-myc), GABA-v3 (GABA.v3-NaVβ1-myc), GABA-v4 (GABA.v4-NaVβ1-myc), AAV-mDlx (mDlx-NaVβ1-myc), and AAV-hSynI (hSynI-NaVβ1-myc) are shown. ITR, inverted terminal repeats (gray boxes); 3′-downstream region (red boxes); RβGpA, rabbit β-globin polyadenylation region (black boxes); TFBS, transcription factor binding site in GABA-v4; WPRE, woodchuck hepatitis virus posttranslational regulatory element.

GABA-v2 was composed of the regulatory element identified by the homology analysis, the mouse *Gad1* minimal promoter,[17] the mouse sodium channel β subunit 1 (*Scn1B* gene coding for NaVβ1), a portion of intron 3, and the 3′-downstream sequence of mouse *Gad1*

Table 1. Semi-quantification of NaVβ1-myc distribution by neonatal i.c.v. + i.c.m. injection

	AAV-mDlx	AAV-hSynI	AAV-v2	AAV-v3	AAV-v4
Injection route	2.5 + 2.5 µL i.c.v.	1 + 1 µL i.c.v. + 3 µL i.c.m.	1 + 1 µL i.c.v. + 3 µL i.c.m.	1 + 1 µL i.c.v. + 3 µL i.c.m.	1 + 1 µL i.c.v. + 3 µL i.c.m.
Viral titer	6.4×10^{13} GC/mL	2.4×10^{13} GC/mL	9.3×10^{13} GC/mL	6.2×10^{13} GC/mL	7.5×10^{13} GC/mL
Total genome copies	3.20×10^{11} GC	1.19×10^{11} GC	4.67×10^{11} GC	3.1×10^{11} GC	3.75×10^{11} GC
No. mice analyzed	3	5	5	5	4
Frontal cortex	+	+++	+++	+	+++
Somatosensory cortex	+	+++	+++	+	++
Visual cortex	−	++	++	−	+
Hippocampus	+ (V)	++	+	−	+
Striatum	+	+++	++	+ (V)	+++
Thalamus	−	++	−	−	−
Hypothalamus	−	++	++	+	++ (V)
Midbrain	−	+	++ (V)	−	+
Cerebellum, GL	−	+	−	−	+
Cerebellum, PL	−	−	−	−	+
Cerebellum, ML	−	−	−	−	−
Pons	−	+	+	−	++
Medulla	−	+	−	−	+

+++, high expression; ++, moderate expression; +, low intensity/sparse expression; −, no expression; (V), brain regions where high intersample (mouse) variability was observed; GL, granule layer; PL, Purkinje layer; ML, molecular layer; GC, genome copies.

(Figure 1D). These DNA components were flanked by inverted terminal repeats for the integration into the rAAV capsid. Intronic 3′-downstream sequences of the mouse *Gad1* gene were used in GABA-v2 as potential regulatory elements for cell-type-specific gene expression.[18,19] To evaluate the activity of the promoter identified by homology analysis alone, intron 3 and the 3′-downstream region of *Gad1* in the GABA-v2 construct were deleted and replaced with the rabbit β-globin polyadenylation region (RβGpA) (GABA-v3; Figure 1D). In GABA-v4, the regulatory elements identified by the TFBS search were used to replace the regulatory elements in GABA-v3 (Figure 1D).

The GABAergic specificity of the GABA-targeting rAAV vectors was compared with a mouse Dlx (mDlx) enhancer, an established GABAergic regulatory element,[8] and the human synapsin I mini-promoter (AAV-hSynI; Figure 1D), which mediates expression in both excitatory and inhibitory neurons.[20,21] To create the mDlx and hSynI constructs, the promoter element in GABA-v3 was replaced with an mDlx promoter to create AAV-mDlx (Figure 1D), and the human synapsin I mini-promoter was used to create AAV-hSynI (Figure 1D). The AAV-hSynI construct contained a woodchuck hepatitis virus posttranslational regulatory element (WPRE) between NaVβ1-myc and RβGpA, which was not present in the other rAAVs. The AAVS used were produced at two vector core facilities (see Materials and methods); titers of the AAVs used ranged from 2.4e13 to 9.3e13 genome copies per milliliter, while the total doses injected ranged from 1.2e11 to 4.6e11 genome copies (Table 1). While this may have been a factor in detecting the transgene in some brain regions of low expression, we believe that it is unlikely that this reasonably narrow range of doses would have a major effect on the cellular specificity.

Mapping of the CNS distribution of transgene expression after neonatal injection

To evaluate transgene expression, the rAAVs were infused to the lateral ventricles by bilateral intracerebroventricular (i.c.v.) and intracisterna magna (i.c.m.) double injections at postnatal day (PND) 2 for widespread dispersion of the rAAV through the CSF. Initially, we injected mDlx in the same manner as the others, 1 µL + 1 µL i.c.v. each side plus 3 µL i.c.m., but we saw almost no expression. Since AAVs using mDlx are operative only in the forebrain and, in our hands, mainly in the hippocampus, we tried injecting 2.5 µL each side i.c.v. only. This resulted in better expression in the forebrain and was sufficient for conducting the double-label experiments.

At PND 30, cortical expression of the NaVβ1-myc transgene was confirmed by immunoblotting using an anti-myc antibody (Figure 2A; note that different exposure times were used for each lane shown). NaVβ1-myc protein was observed between the relative molecular weights of 35–48 kDa (likely corresponding to the glycosylated and unglycosylated forms of NaVβ1)[10,22] in protein lysates from cerebral cortices of mice injected with the GABA-v2, v4, and hSynI vectors. A longer exposure of the immunoblot showed the same banding pattern for AAV-mDlx (Figure 2A). In contrast, transgene expression in the cortex of mice treated with GABA-v3 was not detectable by immunoblotting.

To assess transgene distribution, immunohistochemical analysis was performed using an anti-myc antibody to label NaVβ1-myc-expressing cells. GABA-v2 showed robust transgene expression in multiple brain regions, including the cerebral cortex, striatum (including the
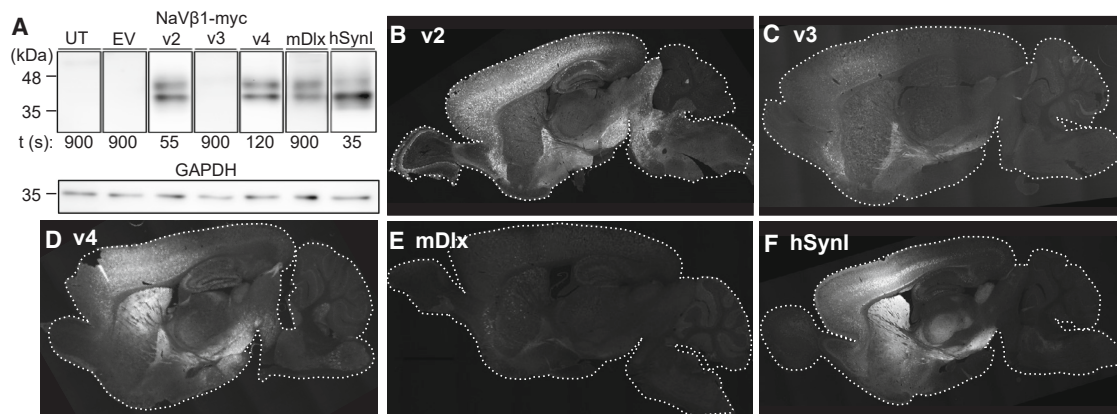
Figure 2. NaVβ1-myc protein expression from rAAVs in mouse brain after i.c.v. + i.c.m. injection at PND 2–3

(A) Immunoblot of NaVβ1-myc expression using an anti-myc antibody in samples of PND 30 mouse cerebral cortex from mice treated with rAAV vectors at PND 2–3. t represents the immunoblot exposure time (seconds) of the individual samples to detect NaVβ1-myc. GAPDH was used as a loading control. UT, untreated; EV, empty vector-treated. (B–F) CNS distributions of GABA-v2 (B; n = 5 mice), v3 (C; n = 5 mice), v4 (D; n = 4 mice), mDlx (E; n = 3 mice), and hSynI (F; n = 5 mice). NaVβ1-myc protein was detected by immunostaining with an anti-myc antibody in brain samples collected at PND 30.

globus pallidus, external segment), hypothalamus, and midbrain; however, transduction of the caudal brain (cerebellum, pons, and medulla) was limited (Figure 2B; Table 1; Figure S2). As expected from the immunoblot result, GABA-v3 showed a substantially lower level of expression in the brain compared with GABA-v2 (Figure 2C; Table 1; Figure S2), with only weak expression in the globus pallidus external segment. This result suggested that the *Gad1* intron 3 and the 3′-downstream sequences are required for the robust expression observed with GABA-v2.

GABA-v4 displayed strong expression in the cortex, with lower expression in the hippocampus and midbrain and higher expression in the striatum compared with GABA-v2 (Figure 2D; Table 1; Figure S2). In addition, GABA-v4 showed low density but consistent transduction of the medulla in the hindbrain and cells within the granule and Purkinje layers of the cerebellar cortex (Figure 2D; Table 1; Figure S2). The selectivities of GABA-v2, v3, and v4 were directly compared with two promoters previously characterized and widely used in rAAVs: AAV-mDlx and AAV-hSynI. By comparison, NaVβ1-myc driven by mDlx was found to be restricted to the forebrain, in agreement with previous findings.[8,9] However, the overall level of transgene expression by AAV-mDlx was very low and sparse in comparison to GABA-v2 and v4 (Figure 2E; Table 1; Figure S2). In contrast, AAV-hSynI displayed robust transduction of the forebrain (such as the cerebral cortex, especially layer 5; striatum; and hippocampus), lower expression in the midbrain, and limited transduction of the hindbrain (Figure 2F; Table 1; Figure S2).

Cell-type specificity and coverage of transgene expression after neonatal injection

To evaluate the cell-type specificity of the expressed transgene, we performed double-label immunohistochemical analyses in samples collected 4 weeks postinjection from the frontal cortex, striatum, hippocampal CA1 region, and hypothalamus at PND 30 using an anti-myc antibody in combination with antibodies for various cell-type markers (Figures 3, S3, and S4). Anti-NeuN was used as a general marker of neurons, while anti-GABA was used to label GABAergic neurons. In the frontal cortex, 90% or more of the myc-expressing cells were also labeled by anti-NeuN for all five vectors, indicating a very high degree of neuronal specificity (Figures 3A–3C) (see "immunohistochemistry analyses and imaging" in the materials and methods for calculation of the cell-type specificity and coverage). GABA-v2 and v4 showed 9.3% and 5.4% coverage, respectively, of frontal cortical NeuN-labeled cells expressing NaVβ1-myc, whereas GABA-v3 and AAV-mDlx showed substantially lower coverage (0.86% and 0.18%, respectively). AAV-hSynI, in comparison, transduced 17% of the neurons (Figure 3D; one-way ANOVA, F = 11.62, p < 0.0001).

In double-labeling experiments, samples collected at PND 30 were co-labeled with anti-myc and anti-GABA antibodies and revealed that GABA-v2, v3, and v4 displayed frontal cortical GABA specificities of 70.7%, 61.5%, and 52.1%, respectively (Figures 3E–3G and S4). AAV-mDlx showed a degree of GABA specificity (68.0%) comparable to those of GABA-v2, v3, and v4 (Figures 3G and S4), whereas AAV-hSynI showed significantly lower specificity (8.7%) than the GABA-targeting rAAVs (Figures 3H and S4; one-way ANOVA, F = 9.796, p < 0.0001). GABA-v2 and v4 displayed 58.1% and 30.2% GABAergic neuronal coverage, respectively. Consistent with the CNS transgene distribution shown in Figure 2, the coverages elicited by GABA-v3 (7.1%) and AAV-mDlx (18.2%) were low. AAV-hSynI (17.0%) displayed an ability to transduce cortical GABAergic neurons comparable to that of AAV-mDlx (18.2%) (Figure 3H).

Analysis of GABA specificity was also performed in the striatum, hippocampal CA1, and hypothalamus (Figure S4). Due to the limited expression of GABA-v3, this construct was excluded from further analysis, and quantification of the AAV-mDlx vector could be
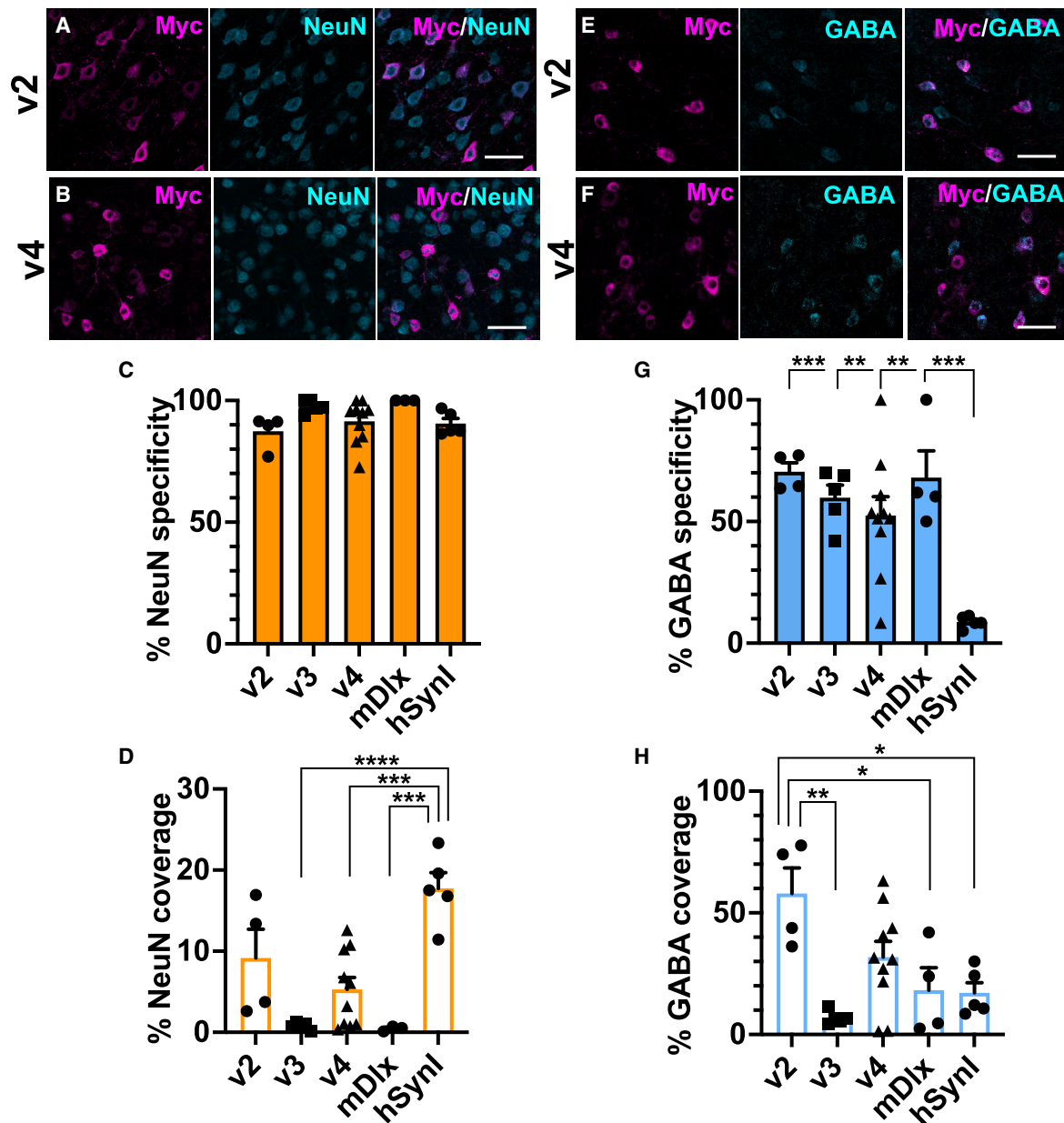
Figure 3. Cell-type specificity and coverage of rAAV vectors in frontal cortex after rAAV injections at PND 2

Immunostaining of NaVβ1-myc (magenta) from GABA-v2 (A) and GABA-v4 (B) using anti-myc and anti-NeuN as a pan-neuronal marker (cyan). Quantitative analysis of transgene expression; NeuN specificity (C) and coverage (D) of the rAAV vectors. Immunostaining of NaVβ1-myc (magenta) from GABA-v2 (E) and GABA-v4 (F) with anti-myc and anti-GABA for GABAergic inhibitory neurons (cyan). Quantitative analysis of GABA specificity (G) and coverage (H) of the rAAV vectors; n = 3–10 mice for each condition. Scale bars, 50 μm. All values are mean ± standard error of the mean. *p < 0.05, **p < 0.01, ***p < 0.001, and ****p < 0.0001, Tukey *post hoc* test.

performed only in the striatum due to insufficient expression in the other regions. Across all brain regions examined, all of the rAAVs showed high NeuN specificity (85% or greater; see Figures S9A, S9E, and S9I), albeit with low coverage (Figures S4, S4B, S4F, and S4J). Therefore, the expression elicited by these GABA-based rAAVs was consistently restricted to neurons across the brain when administered to the neonatal brain.

In the striatum, GABA-v2 showed the highest GABA specificity and coverage (68.5% and 30.9%), whereas GABA-v4 was less specific (specificity 19.7%; coverage 15.2%) (Figure S4). We note that GABA-v2, v3, and v4 all show labeling in the globus pallidus, external segment, consistent with GABAergic neuronal expression (Figure S4). In the CA1 area of the hippocampus, GABA-v2 and v4 showed similar specificities, 57.0% and 60.6%, respectively (Figure S4).
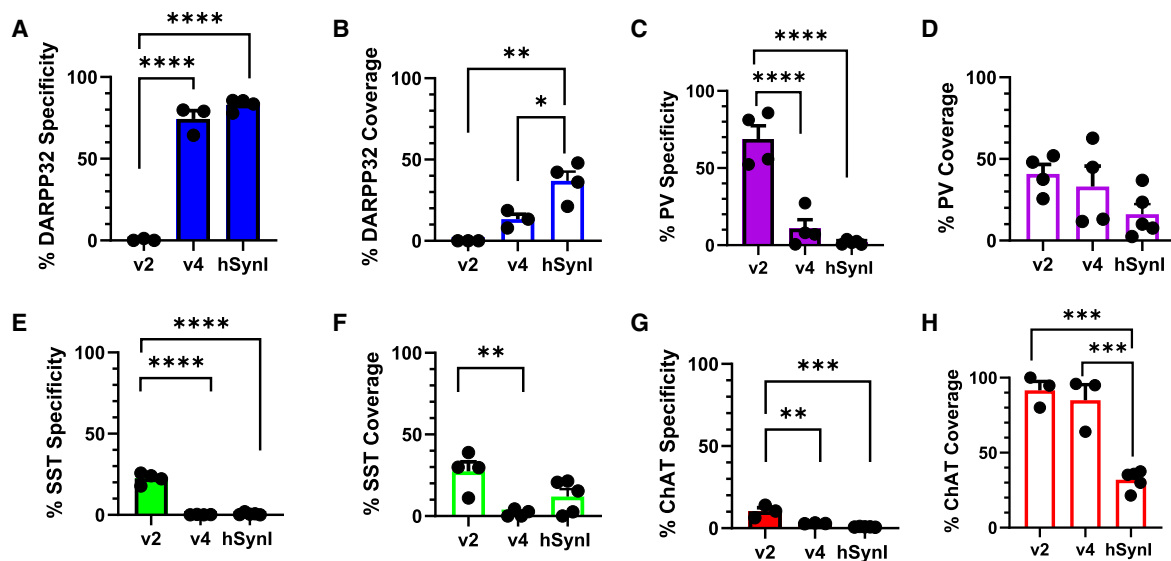
Figure 4. Cell-type specificity of GABA-v2, GABA-v4, and hSynI in the striatum

Mice were injected at PND 2 and brains were collected at PND 30. Quantitative analyses of double labeling of anti-myc and anti-DARPP32 specificity (A) and coverage (B) and PV neuron specificity (C) and coverage (D) are illustrated. SST specificity and coverage are shown in (E) and (F), while ChAT specificity and coverage are shown in (G) and (H). All values are mean ± standard error of the mean; n = 3–5 mice for each cohort. *p < 0.05, **p < 0.01, ***p < 0.001, and ****p < 0.0001, Tukey *post hoc* test.

Although GABA-v2 showed 22.5% GABA coverage, GABA-v4 elicited only 4.3% (Figure S4). The hypothalamic GABA specificities of GABA-v2 and v4 were 33.3% and 24.3%, respectively (Figure S4), and GABA coverages were 28.0% and 12.5% (Figure S4L). These results demonstrate that GABA-v2 and v4 possess very high neuronal specificity and moderate-to-high GABA neuron selectivity in the mouse brain following neonatal injection in the CSF.

Analysis of interneuron subtype selectivity of GABA-v2 and v4 after neonatal injection

Different subclasses of GABAergic interneurons include those that express PV or somatostatin (SST). To examine expression in these classes of neurons, mice were treated by i.c.v. and i.c.m. double injections at PND 2 with GABA-v2 or GABA-v4, and brain samples were collected at PND 30 and immunostained using anti-myc and anti-PV (Figures S5A and S5B) or anti-SST (Figures S5E and S5F) antibodies. In the frontal cortex, GABA-v2 and v4 showed similar PV specificity (Figure S5C; v2, 46.9%; v4, 39.1%), PV coverage (Figure S5D; v2, 52.4%; v4, 31.2%), SST specificity (Figure S5G; v2, 14.8%; v4, 12.4%), and SST coverage (Figure S5H; v2, 71.9%; v4, 47.7%).

We also assessed PV and SST specificity and coverage in the CA1 of the hippocampus (Figures S5I–S5L). While GABA-v4 showed prominent expression in both PV- and SST-expressing neurons (PV, specificity 25.8%, coverage 15.3%; SST, specificity 26.6%, coverage 62.2%), GABA-v2 preferentially transduced SST-expressing neurons (PV, specificity 8.0%, coverage 6.5%; SST, specificity 69.1%, coverage 49.4%) (Figures S5I–S5L). In the hypothalamus, both vectors showed low PV specificity (v2, 8.8%; v4, 6.6%) and moderate coverage (v2, 21.4%; v4, 26.6%) (Figures S5M and S5N). Hypothalam-

ic SST specificity and coverage were not evaluated due to very low SST immunopositivity in this region.

In the striatum, the majority of neurons (95%) are GABAergic medium spiny neurons, which express the marker DARPP32; the remaining 5% comprise various types of interneurons, including PV- and SST-expressing interneurons and GABAergic/cholinergic choline acetyltransferase (ChAT)-positive interneurons.[23] Cellular specificity and coverage analyses of GABA-v2, GABA-v4, and AAV9-hSynI with these neuronal markers were conducted.

Remarkably, the transduction of DARPP32-expressing neurons by GABA-v2 was minimal, whereas GABA-v4 and hSynI primarily expressed in this class of neurons (specificity, v2, 0.4%; v4, 74.4%; hSynI, 83.2%, one-way ANOVA, F = 243.1, p < 0.0001; coverage, v2, 0.03%; v4, 13.3%; hSynI, 36.9%, one-way ANOVA, F = 18.92, p = 0.0015) (Figures 4A and 4B). GABA-v2 showed higher specificity than v4 and hSynI for striatal PV+ interneurons (Figure 4C; v2, 68.8%; v4, 10.7%; hSynI, 1.8%; one-way ANOVA, F = 43.50, p < 0.0001) and for SST+ interneurons (Figure 4E; v2, 22.5%; v4, 0.13%; hSynI, 0.67%; one-way ANOVA, F = 176.4, p < 0.0001). GABA-v2 also showed significantly higher SST coverage than v4, but not hSynI (Figure 4F; v2, 27.4%; v4, 1.76%; hSynI, 12.0%; one-way ANOVA, F = 8.042, p < 0.0083). Both GABA vectors showed a very high propensity (and greater ability overall than hSynI) to transduce ChAT+ interneurons (coverage, v2, 91.6%; v4, 84.9%; hSynI, 32.0%; one-way ANOVA, F = 33.25, p < 0.0001), although ChAT specificities were low (v2, 10.3%; v4, 3.0%; hSynI, 0.79%; one-way ANOVA, F = 24.35, p = 0.0004) (Figures 4G and 4H). Therefore, in the striatum GABA-v2 and GABA-v4 displayed strikingly different patterns of expression;

GABA-v2 was mainly selective for PV-, SST-, and ChAT-expressing interneurons, whereas GABA-v4 was primarily expressed in the DARPP32$^+$ medium spiny neurons.

Characterization of cell-type specificity and coverage of GABA-v2 and GABA-v4 after injection into the adult hippocampus and cerebellum

To assess specificity and coverage in the adult mouse brain, GABA-v2 and v4 were injected into the hippocampus and cerebellum of 2-month old mice and collected 4 weeks later. In the hippocampus, specificity and coverage in the CA1 region was analyzed. GABA-v2 showed sparse transgene expression in the molecular layer and moderate density expression in the pyramidal layer of the CA1, while GABA-v4 showed sparse expression in both layers (Figures 5A and 5B). Double-labeling experiments revealed that (1) GABA-v2 and v4 showed high NeuN specificity (Figure 5C; GABA-v2, 78.7%; GABA-v4, 93.5%), (2) NeuN coverage of GABA-v2 (30.1%) was higher than that of GABA-v4 (18.3%; Figure 5D), and (3) GABA specificity of GABA-v2 (24.7%) was significantly lower than that of GABA-v4 (48.2%; Figure 5G, p < 0.05 by Student's t test), whereas the degrees of GABAergic neuronal coverage of GABA-v2 (46.9%) and GABA-v4 (46.5%) were nearly identical (Figure 5H). The lower GABAergic selectivity of GABA-v2 compared with GABA-v4 suggests that, in the adult hippocampus, NaVβ1-myc expression from GABA-v2 may be targeted to non-GABAergic neurons, such as glutamatergic pyramidal neurons.

Hippocampal cellular selectivity of GABA-v2 and GABA-v4 was also assessed with double labeling using anti-myc in combination with anti-PV and anti-SST (Figures 5I and 5J). PV specificity of GABA-v4 was significantly higher than that of GABA-v2 (Figure 5K; v2, 6.6%; v4, 28.5%; p < 0.001 by Student's unpaired t test). PV coverage and SST selectivity and coverage of GABA-v2 and v4 were similar to each other (Figures 5L, 5M, and 5N; PV coverage, v2, 47.3%; v4, 63.6%; SST specificity, v2, 6.6%; v4, 22.6%; p = 0.061 by Student's unpaired t test; SST coverage, v2, 44.2%; v4, 43.5%). These results further suggest that GABA-v2 also mediates some expression in the non-GABAergic neuronal population in the hippocampus.

GABA specificity of GABA-v2 was lower after adult injections compared with injections made at PND 2 (PND 2, 57.0% vs. 24.7% in the adult hippocampal CA1; p = 0.016 by unpaired Student's t test, t = 3.02, df = 8), while GABA specificity of GABA-v4 was roughly comparable between the adult and the PND 2 injections (PND 2, 60.6% vs. 48.2% in the adult CA1).

The cerebellum displayed relatively low transduction after PND 2 injection of GABA-v2 and v4 (Table 1). Therefore, to further characterize promoter activity, these rAAVs were injected into the adult cerebellum (the site of injection is illustrated schematically in Figure S6). Strong localized transduction was observed in the cerebellum in mice injected with GABA-v2 and v4 (Figure 6). Cellular specificity and coverage of cerebellar GABAergic neurons were quantified by immunostaining with an anti-my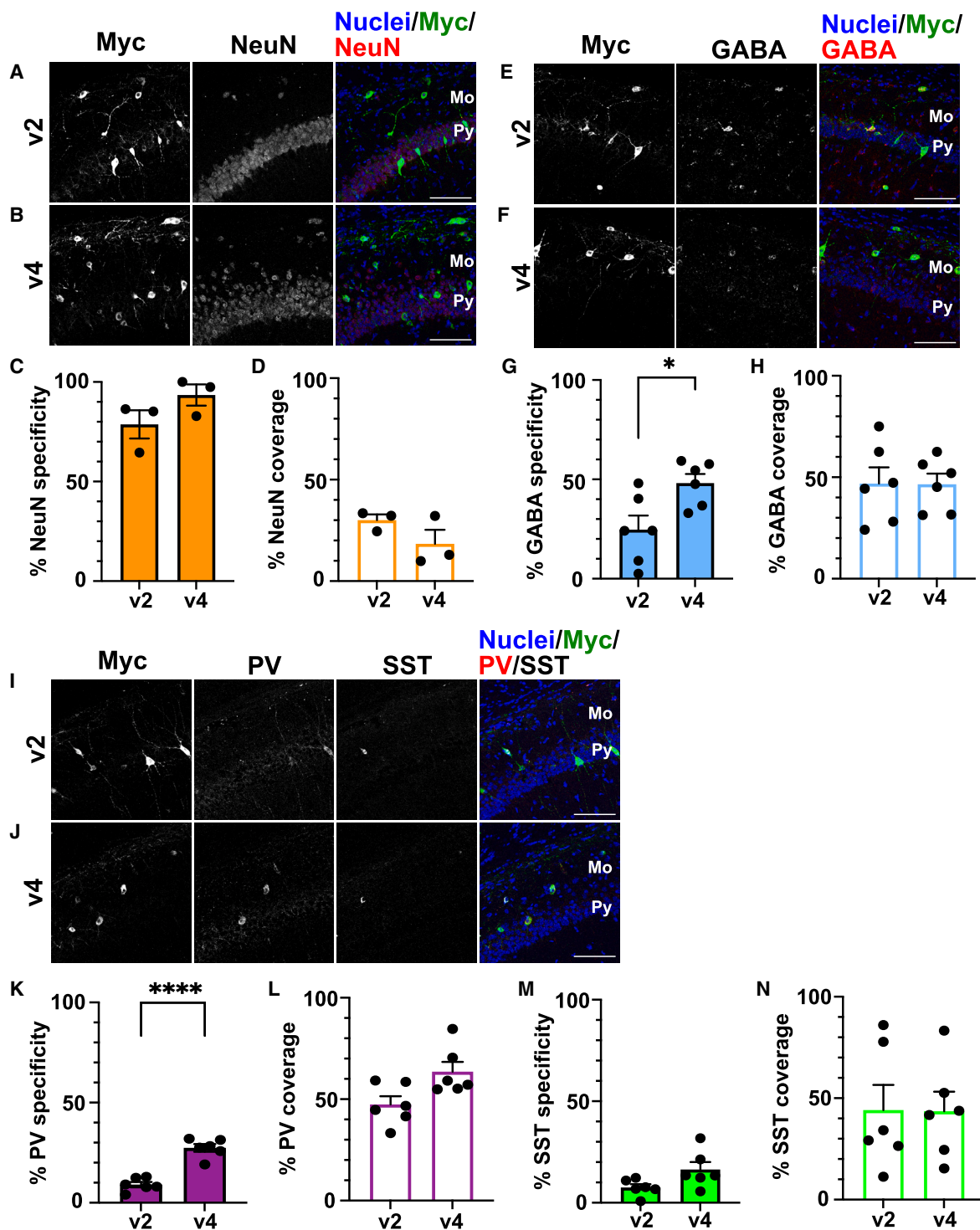c antibody in combination with anti-calbindin-28K for marking Purkinje neurons (Figure 6A) or with anti-PV for basket and stellate cells in the molecular cell layer, as well as Purkinje neurons (Figure 6B). Double-labeling analyses revealed that GABA-v4 showed higher calbindin (Purkinje neuron) specificity and coverage than GABA-v2 (calbindin specificity, GABA-v2, 2.2%; GABA-v4, 12.5%; calbindin coverage, GABA-v2, 6.4%; GABA-v4, 30.0%; Figures 6C and 6D). PV specificity and coverage of GABA-v4 were moderate (specificity, 36.3%; coverage, 36.0%) and higher than those of GABA-v2 (specificity, 8.7%; coverage, 10.2%; Figures 6E and 6F). Inhibitory Golgi neurons are large cells that are sparsely distributed among the glutamatergic granule neurons in the granule cell layer.[24] Large myc-positive cells in the granule cell layer of mice injected with GABA-v2 and GABA-v4 were sparsely distributed in the granule layer; the pattern of immunolabeling strongly suggested that these were inhibitory Golgi neurons (Figures 6G and 6H). Overall, these results indicated that GABA-v2 and GABA-v4 in the adult cerebellum have different patterns of expression and that GABA-v4 showed higher cerebellar GABAergic selectivity than GABA-v2.

DISCUSSION

Strategies for the selection of rAAV-compatible gene-regulatory elements

A major challenge in discovering regulatory elements (transcriptional promoters, enhancers, and suppressors) for use in rAAVs is the identification of the key stretches of genomic DNA that mediate cell-type specificity and subsequently arranging and condensing these sequences into smaller DNA segments that can be used to drive recombinant transgene expression within the limited space available in rAAV vectors (maximum 4.7 kb for single-stranded rAAV vectors and 2.3 kb for self-complementary rAAVs). To identify the regulatory elements from long genomic DNA sequences, we used three types of *in silico* analyses. The first, used previously by Niibori et al.,[10] was straightforward: promoter selection by truncation of the genomic DNA upstream of the transcription start site. In the context of the *Gad1* gene, a 2.7-kb segment of the 5′ upstream region (which we call GABA-v1) showed high neuron specificity (90% based on NeuN co-immunolabeling), but relatively low GABA selectivity (30% or less).[10] The second strategy was to identify genomic DNA sequences conserved among mammalian species in GABA-linked genes; this approach was used to create GABA-v2, which included conserved sequences in both the 5′ upstream and the 3′ downstream regions of the mouse *Gad1* gene. The GABA-v3 construct was identical to GABA-v2 but did not contain the conserved 3′ downstream sequence in *Gad1*. The third strategy utilized TFBS analyses whereby multiple conserved GABA gene-linked sequences were combined into a single rAAV construct to create GABA-v4.

We performed TFBS prediction using JASPAR datasets to develop the GABA-v4 promoter (Figure 1). However, this approach may not effectively exclude false-positive TFBSs from the selection. An alternative strategy to minimize false-positive TFBS candidates is to identify the TFBS-bound transcription factors *in vivo* by chromatin immunoprecipitation-sequencing (ChIP-seq) datasets from the

Figure 5. NeuN and GABA specificity and coverage after adult hippocampal injections

Brain sections were collected 28 days postinjection and the CA1 region was analyzed. Double-labeling immunostaining of NaVβ1-myc from GABA-v2 (A, E, and I) and GABA-v4 (B, F, and J) with anti-myc and anti-NeuN (A and B), anti-GABA (E and F), or anti-PV and SST (I and J) antibodies in the CA1. Quantitative analysis of NeuN specificity (C), NeuN coverage (D), GABA specificity (G), GABA coverage (H), PV and SST specificity (K and M), and PV and SST coverage (L and N) with GABA-v2 and GABA-v4 in the CA1. Scale bars, 100 μm. Values are means ± standard errors of the mean; n = 6 mice for PV and SST and n = 3 for NeuN. Mo, molecular layer; Py, pyramidal cell layer. *p < 0.05, ****p < 0.0001, unpaired t test.
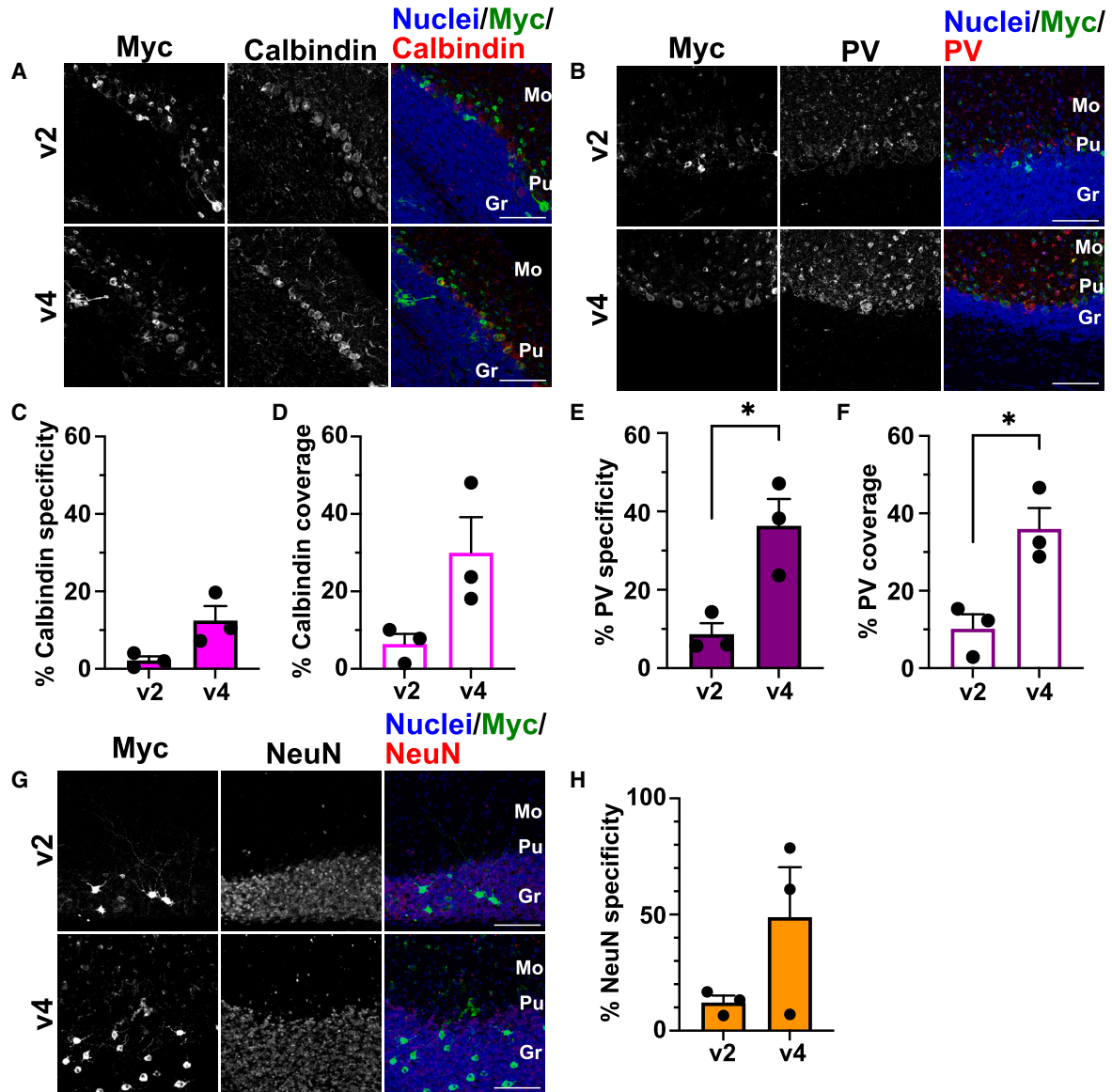
Figure 6. Double-label analysis of calbindin, PV, and NeuN specificity and coverage after injection of GABA-v2 and -v4 into the adult mouse cerebellum

Representative examples of immunostaining of NaVβ1-myc of GABA-v2 and GABA-v4 with anti-myc and anti-calbindin antibodies (A) and anti-myc and anti-PV (B). Quantitative analysis of calbindin cellular specificity (C) and coverage (D) and PV specificity (E) and coverage (F). (G) Immunostaining with anti-myc and anti-NeuN antibodies. (H) Quantitative analysis of NeuN cellular specificity. Scale bars, 100 μm. Values are means ± standard errors of the mean; n = 3 mice for each analysis. Mo, molecular layer; Pu, Purkinje cell layer; Gr, granule cell layer. *p < 0.05, unpaired t test.

UniBind or ENCODE portal.[25,26] Although there are limitations to the availability of the transcription factors in these databases, this approach and others (e.g., Lawler et al.[27]) may allow elimination of the false-positive TFBSs. Another tactic would be to increase the number of non-GABAergic neuronal genes used in the GABA-v4 promoter design. In this study, the Camk2a gene is used as the only non-GABAergic gene. However, the Camk2a promoter is selective for, but not entirely specific for, glutamatergic neurons,[28] and therefore the use of additional non-GABAergic genes (e.g., *vGlut1* or *Iba1*)

to further exclude TFBS candidates may further eliminate other false-positive TFBSs. More stringent exclusion of false-positive TFBSs from the GABA-v4 promoter may contribute not only to decreasing the size of the promoter, but also to increasing the cell-type specificity.

Factors affecting the CNS distributions and GABAergic neuronal selectivities of the rAAVs

Initial *in vivo* assessments of the efficacies of the novel GABA promoters were performed following rAAV9 treatment on PND 2.

Injection of rAAVs into the CSF at this early postnatal stage was done to facilitate widespread vector dispersion in the CNS. We and others have shown that intra-CSF injections of rAAVs in the mouse and rat CNS on PND 2 or 3 results in superior brain-wide distribution compared with intra-CSF injections made at later time points (e.g., see Gholizadeh et al.,[29] Arsenault et al.,[21] Hampson et al.,[30] and Hooper et al.[31]). A direct comparison was made among our novel GABA-based vectors with an rAAV using the mDlx enhancer element for GABA neuron-selective expression and an rAAV9 containing the human synapsin I promoter for general neuronal expression.

Our findings demonstrate that after PND 2 injection into the CSF, GABA-v2 and v4 showed broad brain distribution of the expressed transgene protein and modest-to-high GABA selectivity (20%–70%). The mDlx promoter has previously been reported to convey high GABA specificity after rAAV injection into adult cerebral cortex or hippocampus (90% or more).[8,9] However, we found that after PND 2 CSF injection of the mDlx construct, the level of transgene expression was low, and the brain distribution was limited to small populations of neurons in the mouse forebrain.

In contrast, expression from GABA-v2 and v4 was observed in the forebrain, midbrain, hindbrain, and cerebellum. This observation is consistent with the fact that the *Gad1* gene encoding the Gad-67 form of the enzyme is expressed in GABAergic neurons throughout the brain. *Gad1*-expressing neurons encompass a wide variety of GABAergic neuronal subtypes, each of which shows different firing properties and distinct transcriptional expression profiles.[32,33] This raises the possibility that *Gad1* gene expression may be regulated by different transcription mechanisms in different cell types.

Notably, we found that, following neonatal administration of GABA-v2, transgene expression in the striatum almost entirely precluded GABAergic medium spiny neurons and was largely restricted to interneurons. This finding suggests that regulation of the expression of *Gad1* in striatal spiny neurons differs from that in striatal interneurons and may be regulated by genetic elements not found in GABA-v2. Interestingly, expression by GABA-v4 in the striatum following the same treatment was almost entirely absent in SST⁺ interneurons and was mainly found in medium spiny neurons and PV⁺ interneurons, further illustrating potential differences in the regulation of expression of GABAergic genes between neuronal subclasses.

We also sought to compare the cell-type specificity of the rAAVs at PND 2 after intra-CSF injections made directly into adult mouse brain. Of particular interest was an assessment of activity in the hippocampus and cerebellum, as perturbations in GABA neuronal functions in these regions are associated with disease states such as epilepsy, autism, and schizophrenia.[5,24,34,35]

Intrahippocampal and intracerebellar injections of GABA-v4 in adult mice showed strong transgene expression and moderate GABA selectivity, which was comparable to the level of GABA selec-

tivity seen after neonatal intra-CSF injection. In contrast, administration of GABA-v2 into the adult parenchyma displayed somewhat lower GABA selectivity relative to neonatal CSF treatment. Expression mediated by GABA-v2 in the hippocampus appeared to be present in some glutamatergic neurons, and thus, the GABA-v2 promoter may encode regulatory elements that activate transcription in glutamatergic neurons. One explanation for dual expression in both GABAergic and glutamatergic neurons may be that the transcription factors are expressed in both neuronal types. For example, CREB, REST, and EGR are transcription factors that are expressed in both glutamatergic and GABAergic neurons.[36–39]

The findings from this study demonstrate that it is possible to generate GABA promoters that differ greatly in the level of expression across the CNS and in the degree of GABA neuron-subtype selectivity. In particular, the high GABA neuron selectivity of the GABA-v4 construct illustrates the utility of creating novel gene-regulatory elements that do not naturally exist in genomes. Importantly, the *in silico* methods developed here for the study of GABA-selective promoters are applicable to the identification of rAAV-compatible gene-control elements in other genes. These approaches could be combined with datasets for RNA expression, the binding of transcription-regulatory proteins, and the use of three-dimensional genomic structures to develop other novel gene-regulatory elements with high cell-type specificity and broad CNS expression.

MATERIALS AND METHODS
Acquisition of 5′ intergenic sequences of neuronal genes
The genomic DNA sequences between the 5′ end of the coding regions of neural genes (*Gad1*, *Gad2*, *Slc32a1*, and *Camk2a* genes) and the 3′ end of their 5′-upstream genes (*Erich2*, *Myo3a*, *Arhgap40*, and *Arsi* genes) were obtained from the human (hg38) and mouse (mm10) genome sequences in the UCSC Genome Browser.

The locations of the 5′-upstream sequences for each gene are as follows: human *GAD1*, from 170,798,894 to 170,818,592 on chromosome 2; mouse *Gad1*, from 70,540,811 to 70,563,832 on chromosome 2; human *GAD2*, from 26,211,963 to 26,216,810 on chromosome 10; mouse *Gad2*, from 22,618,169 to 22,622,663 on chromosome 2; human *SLC32A1*, from 38,649,848 to 38,724,725 on chromosome 20; mouse *Slc32a1*, from 158,550,628 to 158,611,242 on chromosome 2; human *CAMK2A* (minus strand), from 150,289,625 to 150,297,214 on chromosome 5; mouse *Camk2a*, from 60,917,768 to 60,925,779 on chromosome 18.

Homology analysis
A pairwise alignment was performed on human and mouse *Gad1* 5′-upstream sequences by the LAGAN alignment program,[14] and the sequence identity was visualized by the VISTA program.[40] The length of the sequence window was 100 bases, and the number of the homologous nucleotides between the two sequences out of 100 bases was calculated as the percentage identity. DNA sequences with more than 70% identity in the mouse *Gad1* 5′-upstream sequence were extracted and ligated sequentially from the 5′ end.

Transcription factor binding site prediction

TFBSs in human and mouse *Gad1*, *Gad2*, *Slc32a1*, and *Camk2a* 5′-upstream sequences were predicted by the motifs module of Biopython using position-specific scoring matrices (PSSMs) converted from the position-frequency matrices of non-redundant vertebrate transcription factor binding profiles in the JASPAR CORE 2018 database.[15] The GC content for the calculation of the position-weight matrices and the PSSMs was 40%. The threshold of the TFBS prediction by PSSM used employed a balanced threshold (1,000). The TFBS sequences conserved in both species and overlapping among three GABA genes—*Gad1*, *Gad2*, and *Slc32a1*—were extracted. Then, TFBSs present in the *Camk2a* gene, a gene primarily expressed in glutamatergic neurons,[41] were subtracted from the TFBSs conserved in the three GABAergic genes. The TFBSs specific to the GABAergic genes were identified on mouse *Gad1* 5′-upstream sequence, extracted, and ligated from the 5′-end sequentially. These custom gene promoters were ligated to the coding region of the mouse *Scn1b* gene as described previously.[10] The GenBank accession numbers for the promoters described in this paper (Figure 1D) are GABA-v2, OQ348122; GABA-v3, OQ348123; GABA-v4, OQ348124; mDlx, OQ348125; and hSyn, OQ348126.

AAV vector generation and virus production

GABA-v2 was composed of the DNA fragments of (1) inverted terminal repeats (ITRs; all constructs used ITRs from AAV2), (2) high DNA sequence identity from the mouse genome, (3) the mouse *Gad1* minimal promoter, (4) the mouse *Scn1b* gene encoding NaVβ1 protein fused to a c-myc tag at the C terminus (NaVβ1-myc), (5) a part of intron 3 of mouse *Gad1*, (6) the mouse *Gad1* 3′-downstream sequence, and (7) a second ITR. These DNA fragments were arranged in a tandem manner. The DNA sequences between the ITRs of GABA-v2, GABA-v3, and GABA-v4 were synthesized and cloned in the pMA vector by GeneArt (Thermo Fisher). pAAV-mDlx-GFP and hSynI-FMR1-WPRE were obtained from Addgene and the University of Pennsylvania Vector Core, respectively. The GFP and WPRE in AAV-mDlx-GFP and fmr1 cDNA in hSynI-FMR1-WPRE were replaced with NaVβ1-myc amplified from pAAV-Gad.v1-NaVβ1-myc by PCR using TopTaq DNA polymerase (Qiagen).[10] The primer set for NaVβ1-myc amplification was (1) forward, 5′-gtcaGAATTCgatcGCTAGCcgatgc caccATGGGGACGCTGCTGGCTCTCG-3′, and (2) reverse, 5′-gcatG GATCCacgtTCACAGATCCTCTTCTGAGATGAG-3′. The plasmids were amplified and purified by endotoxin-free Maxi-Prep (Qiagen) for AAV9 production.

AAV particles were manufactured at the University of Pennsylvania Vector Core (GABA-v4-NaVβ1) and at Vigene Biosciences (GABA-v2-NaVβ1, GABA-v3-NaVβ1, mDlx-NaVβ1, Synapsin-NaVβ1) and were purified using iodixanol gradient ultracentrifugation to remove impurities and empty capsids. Viral titers were determined using qPCR (Vigene) or digital drop PCR (University of Pennsylvania) with quantification based on the ITRs present in the viral genome. All mice were injected with viruses containing AAV9 capsids.

Mice and neonatal cerebrospinal fluid injections

C57BL/6J wild-type (B6) mice and 129S6/SvEvTac Scn1a heterozygous (129S Scn1a+/−) mice were obtained from The Jackson Laboratory. Male 129S Scn1a+/− mice were crossed with female B6 mice to generate 129S × B6 F1 hybrid Scn1a+/− (F1 Scn1a+/−) and wild-type (F1 WT) littermate offspring. The mice were kept on a 06:00–20:00 light/dark cycle with *ad libitum* access to water and food. All animal protocols and procedures were approved by the University of Toronto Animal Care Committee. The mice were injected with GABA-v2 (2 × B6 mice and 2 × F1 WT mice), GABA-v3 (5 × F1 WT mice), GABA-v4 (7 × F1 WT mice and 3 × F1 Scn1a+/− mice), AAV9-mDlx (4 × F1 WT mice), or AAV9-hSynI (5 × F1 WT mice) via bilateral i.c.v. and i.c.m. routes at PND 2 as described by Niibori et al..[10] The needle was placed at 1 mm anterior from lambda and 1 mm lateral from the midline for i.c.v. injection and 2 mm posterior from lambda along the midline for i.c.m. injection. The injection needles were custom-made from 30G needles and were connected to a Quintessential stereotaxic injector (Stoelting) through high-performance liquid chromatography (HPLC) tubing. The cut edge of the needle was placed facing posterior for i.c.v. injection and toward the ventral side for i.c.m. injection. Five microliters of AAV vector (1 µL/side bilaterally for i.c.v. injection, plus 3 µL for i.c.m. injection for GABA-v2, v3, v4, and hSynI and 2.5 µL/side bilateral i.c.v. for AAV9-mDlx) was infused at a flow rate of 1 µL/min. The needle was kept in place for an additional minute after the infusion. rAAV9 doses ranged from 1.19×10^{11} to 4.67×10^{11} genome copies (GCs) for GABA-v2, 3.10×10^{11} GCs for GABA-v3, 3.75×10^{11} GCs for GABA-v4, 3.20×10^{11} GCs for AAV-mDlx, and 1.19×10^{11} GCs for AAV-hSynI (see Table 1).

Adult parenchymal injection

Sixty to eighty-day-old C57BL/6J mice were administered 1 µL of rAAV (1×10^{13} GC/mL) into the hippocampus or cerebellum by stereotaxic injection. The mice were anesthetized with a mixture of ketamine (150 mg/kg) and xylazine (10 mg/kg) in saline solution by intraperitoneal injection. The coordinates for the hippocampal injection were 2 mm posterior from the bregma, 1.8 mm lateral from the midline, and 1.5 mm deep from the bregma, and the coordinates for the cerebellar injection were 6 mm posterior from the bregma, 1.8 mm lateral from the midline, and 2 mm deep from the bregma. rAAVs were injected with a sterilized Hamilton syringe (no. 702) at a flow rate of 0.1 µL/min. The needle was left in place for an additional minute after the infusion. The incisions were sutured after administration of meloxicam (2 mg/kg), and the mice were allowed to recover on a heating pad.

Immunoblotting

The cerebral cortices from PND 29–32 mice were dissected, frozen on dry ice, and stored at −80°C until processing. Cortical hemispheres were added to 1 mL homogenization buffer (0.05 M Tris, 1% SDS, 1× cOmplete mini-protease inhibitor [Roche Diagnostics], pH 7.4–7.6) and were homogenized using a Heidolph homogenizer. Total protein concentration was measured using the Pierce BCA assay kit

(23227; Thermo Scientific). Samples were diluted to 1 mg/mL in sample buffer containing 2 M urea, 1× NuPAGE LDS sample buffer (Invitrogen), and 0.1 M dithiothreitol (Bioshop) and incubated at 37°C for 20 min. Ten micrograms of protein was loaded per lane and resolved on 10% SDS-polyacrylamide gels, transferred to a nitrocellulose membrane, and blocked for 1 h at room temperature with 5% skim milk diluted in wash buffer (1 mM Tris, 150 mM NaCl, 0.2% Tween 20 in distilled water). Primary antibodies were applied to the membranes (rabbit anti-myc [1:3,000; Abcam], diluted in 5% skim milk in wash buffer; rabbit anti-GAPDH [1:2,000; Abcam], diluted in 5% bovine serum albumin in wash buffer) and incubated overnight at 4°C. After washing, the membranes were incubated for 2 h at room temperature in secondary antibody (goat anti-rabbit IgG horseradish peroxidase conjugated [1:3,000; Jackson ImmunoResearch], diluted in 2% skim milk in wash buffer). Membranes were imaged using the SuperSignal West Pico PLUS Chemiluminescent Substrate Kit (Thermo Scientific) and ChemiDoc Image System (Bio-Rad).

Immunohistochemistry analyses and imaging

Mice ages PND 29–32 were anesthetized by intraperitoneal injection of ketamine/xylazine solution and transcardially perfused with 1× phosphate-buffered saline (PBS), fixed in 4% paraformaldehyde (PFA) in 1× PBS, and postfixed in 4% PFA at 4°C overnight. The brains were immersed in 30% sucrose solution for 1–3 days and then frozen on dry ice with O.C.T. Compound medium (Fisher Healthcare). Twenty-micrometer-thick brain slices in the sagittal plane were cut using a Leica CM3050 S cryostat and were stored at 4°C in PBS. Unless otherwise specified, all of the following steps were conducted at room temperature. Brain slices were incubated in 1% Triton X-100 for 30 min, incubated in blocking buffer (5% bovine serum albumin, 5% normal donkey serum in 1× PBS) for 1 h, and then incubated in primary antibody diluted in blocking buffer solution overnight at 4°C. The primary antibody used for qualitative distribution analyses of the NaVβ1-myc transgene was rabbit anti-myc (1:4,000, ab9106; Abcam). For quantitative double-label analyses, the primary antibodies used were rabbit anti-GABA (1:1,000, A2052; Sigma-Aldrich), rabbit anti-NeuN (1:9,000, ab177487; Abcam), rabbit anti-PV (1:1,000, ab11427; Abcam), rat anti-SST (1:100, MAB354; Millipore Sigma), and mouse anti-calbindin 28-K (1:1,000, C9848; Sigma-Aldrich). The slices were incubated in secondary antibody diluted in 5% donkey serum in 1× PBS for 2 h. Secondary antibodies used were donkey anti-rabbit Alexa Fluor 594 (1:2,000, A21207; Invitrogen) and goat anti-rat Alexa Fluor 647 (1:3,000, A21247; Invitrogen). Sections were washed again five times. For quantitative double-label analyses, the following intermediate steps were performed at this stage: rabbit anti-myc antibody (Abcam ab9106) was conjugated to Alexa Fluor 488 fluorophore using the Alexa Fluor 488 antibody labeling kit (Thermo Fisher Scientific), diluted in blocking buffer 1:1,000, incubated with the slices overnight at 4°C, and then incubated in DAPI (5 μg/mL in 1× PBS) for 20 min, washed once with 1× PBS, mounted on microscope slides, air dried, and covered in Prolong Gold Antifade Solution (Invitrogen).

For qualitative transgene distribution analysis, tiled images of brain slices stained with rabbit anti-myc were taken at 4× magnification of an area encompassing the entirety of each section using a Cytation5 slide scanner (Bio-Rad) (maintained by the Center for Pharmaceutical Oncology, Leslie Dan Faculty of Pharmacy, University of Toronto). The images were stitched to give a single image of the section. Images were taken of sagittal sections approximately 1, 2, and 3 mm from the midline for analysis. Semi-quantitative scoring of transgene expression in selected brain regions was performed by gating the background signal in ImageJ Fiji relative to untreated negative controls.

For quantitative cell specificity analysis, images of double-labeled brain slices (two slices per mouse) were obtained at 20× magnification using an LSM700 confocal microscope (Zeiss). Image analysis and cell counting were performed using ImageJ Fiji. Specificity was calculated as the number of cells with overlapping NaVβ1-myc-expressing cells and cell-type marker-expressing cells divided by the number of total cells with NaVβ1-myc-expressing cells, multiplied by 100%, whereas coverage was calculated as the number of cells with overlapped cells divided by the total number of cells with cell-type-expressing cells multiplied by 100%.

Statistical analyses

Data comparing two groups were analyzed with a two-tailed, unpaired t test, while data with more than two groups were analyzed by one-way analysis of variance (ANOVA, followed by Tukey's *post hoc* test. The results are presented as the mean ± standard error of the mean.

DATA AVAILABILITY

Data are available upon request.

SUPPLEMENTAL INFORMATION

Supplemental information can be found online at https://doi.org/10.1016/j.omtm.2023.01.007.

AUTHOR CONTRIBUTIONS

Y.N., J.B.S., and D.R.H. conceived the project; Y.N. and R.D.-K. conducted the laboratory work; Y.N., R.D.-K., and D.R.H. analyzed the data; and all authors discussed the data. Y.N., R.D.-K., and D.R.H. wrote the first draft of the paper and all other authors provided comments.

DECLARATION OF INTERESTS

J.B.S. and J.T.B. declare that they own stock in and are employees of REGENXBIO, Inc.

REFERENCES

1. Dravet, C. (2011). The core Dravet syndrome phenotype: core Dravet Syndrome. Epilepsia *52*, 3–9. https://doi.org/10.1111/j.1528-1167.2011.02994.x.

2. Paluszkiewicz, S.M., Martin, B.S., and Huntsman, M.M. (2011). Fragile X syndrome: the GABAergic system and circuit dysfunction. Dev. Neurosci. *33*, 349–364. https://doi.org/10.1159/000329420.

3. Soghomonian, J.-J., Zhang, K., Reprakash, S., and Blatt, G.J. (2017). Decreased parvalbumin mRNA levels in cerebellar Purkinje cells in autism: cerebellar parvalbumin expression. Autism Res. *10*, 1787–1796. https://doi.org/10.1002/aur.1835.

4. Lang, U.E., Puls, I., Müller, D.J., Strutz-Seebohm, N., and Gallinat, J. (2007). Molecular mechanisms of schizophrenia. Cell. Physiol. Biochem. *20*, 687–702. https://doi.org/10.1159/000110430.

5. Yu, F.H., Mantegazza, M., Westenbroek, R.E., Robbins, C.A., Kalume, F., Burton, K.A., Spain, W.J., McKnight, G.S., Scheuer, T., and Catterall, W.A. (2006). Reduced sodium current in GABAergic interneurons in a mouse model of severe myoclonic epilepsy in infancy. Nat. Neurosci. *9*, 1142–1149. https://doi.org/10.1038/nn1754.

6. Kalume, F., Oakley, J.C., Westenbroek, R.E., Gile, J., de la Iglesia, H.O., Scheuer, T., and Catterall, W.A. (2015). Sleep impairment and reduced interneuron excitability in a mouse model of Dravet Syndrome. Neurobiol. Dis. *77*, 141–154. https://doi.org/10.1016/j.nbd.2015.02.016.

7. Cleary, C.M., Milla, B.M., Kuo, F.-S., James, S., Flynn, W.F., Robson, P., and Mulkey, D.K. (2021). Somatostatin-expressing parafacial neurons are CO2/H+ sensitive and regulate baseline breathing. Elife *10*, e60317. https://doi.org/10.7554/eLife.60317.

8. Dimidschstein, J., Chen, Q., Tremblay, R., Rogers, S.L., Saldi, G.-A., Guo, L., Xu, Q., Liu, R., Lu, C., Chu, J., et al. (2016). A viral strategy for targeting and manipulating interneurons across vertebrate species. Nat. Neurosci. *19*, 1743–1749. https://doi.org/10.1038/nn.4430.

9. Mehta, P., Kreeger, L., Wylie, D.C., Pattadkal, J.J., Lusignan, T., Davis, M.J., Turi, G.F., Li, W.-K., Whitmire, M.P., Chen, Y., et al. (2019). Functional access to neuron subclasses in rodent and primate forebrain. Cell Rep. *26*, 2818–2832.e8. https://doi.org/10.1016/j.celrep.2019.02.011.

10. Niibori, Y., Lee, S.J., Minassian, B.A., and Hampson, D.R. (2020). Sexually divergent mortality and partial phenotypic rescue after gene therapy in a mouse model of Dravet syndrome. Hum. Gene Ther. *31*, 339–351. https://doi.org/10.1089/hum.2019.225.

11. Hoshino, C., Konno, A., Hosoi, N., Kaneko, R., Mukai, R., Nakai, J., and Hirai, H. (2021). GABAergic neuron-specific whole-brain transduction by AAV-PHP.B incorporated with a new GAD65 promoter. Mol. Brain *14*, 33. https://doi.org/10.1186/s13041-021-00746-1.

12. Vormstein-Schneider, D., Lin, J.D., Pelkey, K.A., Chittajallu, R., Guo, B., Arias-Garcia, M.A., Allaway, K., Sakopoulos, S., Schneider, G., Stevenson, O., et al. (2020). Viral manipulation of functionally distinct interneurons in mice, non-human primates and humans. Nat. Neurosci. *23*, 1629–1636. https://doi.org/10.1038/s41593-020-0692-9.

13. Duba-Kiss, R., Niibori, Y., and Hampson, D.R. (2021). GABAergic gene regulatory elements used in adeno-associated viral vectors. Front. Neurol. *12*, 745159.

14. Brudno, M., Do, C.B., Cooper, G.M., Kim, M.F., Davydov, E., NISC Comparative Sequencing Program, Green, E.D., Sidow, A., and Batzoglou, S. (2003). LAGAN and multi-LAGAN: efficient tools for large-scale multiple alignment of genomic DNA. Genome Res. *13*, 721–731. https://doi.org/10.1101/gr.926603.

15. Khan, A., Fornes, O., Stigliani, A., Gheorghe, M., Castro-Mondragon, J.A., van der Lee, R., Bessy, A., Chèneby, J., Kulkarni, S.R., Tan, G., et al. (2018). Jaspar 2018: update of the open-access database of transcription factor binding profiles and its web framework. Nucleic Acids Res. *46*, D260–D266. https://doi.org/10.1093/nar/gkx1126.

16. Ansari, A.M., Ahmed, A.K., Matsangos, A.E., Lay, F., Born, L.J., Marti, G., Harmon, J.W., and Sun, Z. (2016). Cellular GFP toxicity and immunogenicity: potential confounders in in vivo cell tracking experiments. Stem Cell Rev. Rep. *12*, 553–559. https://doi.org/10.1007/s12015-016-9670-8.

17. Chen, Y., Dong, E., and Grayson, D.R. (2011). Analysis of the GAD1 promoter: trans-acting factors and DNA methylation converge on the 5′ untranslated region. Neuropharmacology *60*, 1075–1087. https://doi.org/10.1016/j.neuropharm.2010.09.017.

18. Yan, H., Tang, G., Wang, H., Hao, L., He, T., Sun, X., Ting, A.H., Deng, A., and Sun, S. (2016). DNA methylation reactivates GAD1 expression in cancer by preventing CTCF-mediated polycomb repressive complex 2 recruitment. Oncogene *35*, 3995–4008. https://doi.org/10.1038/onc.2015.423.

19. Niibori, Y., Hayashi, F., Hirai, K., Matsui, M., and Inokuchi, K. (2007). Alternative poly(A) site-selection regulates the production of alternatively spliced vesl-1/homer1 isoforms that encode postsynaptic scaffolding proteins. Neurosci. Res. *57*, 399–410. https://doi.org/10.1016/j.neures.2006.11.014.

20. McLean, J.R., Smith, G.A., Rocha, E.M., Hayes, M.A., Beagan, J.A., Hallett, P.J., and Isacson, O. (2014). Widespread neuron-specific transgene expression in brain and spinal cord following synapsin promoter-driven AAV9 neonatal intracerebroventricular injection. Neurosci. Lett. *576*, 73–78. https://doi.org/10.1016/j.neulet.2014.05.044.

21. Arsenault, J., Gholizadeh, S., Niibori, Y., Pacey, L.K., Halder, S.K., Koxhioni, E., Konno, A., Hirai, H., and Hampson, D.R. (2016). FMRP expression levels in mouse central nervous system neurons determine behavioral phenotype. Hum. Gene Ther. *27*, 982–996. https://doi.org/10.1089/hum.2016.090.

22. Kruger, L.C., O'Malley, H.A., Hull, J.M., Kleeman, A., Patino, G.A., and Isom, L.L. (2016). β1-C121W is down but not out: epilepsy-associated *Scn1b-C121W* results in a deleterious gain-of-function. J. Neurosci. *36*, 6213–6224. https://doi.org/10.1523/JNEUROSCI.0405-16.2016.

23. Matamales, M., Bertran-Gonzalez, J., Salomon, L., Degos, B., Deniau, J.-M., Valjent, E., Hervé, D., and Girault, J.-A. (2009). Striatal medium-sized spiny neurons: identification by nuclear staining and study of neuronal subpopulations in BAC transgenic mice. PLoS One *4*, e4770. https://doi.org/10.1371/journal.pone.0004770.

24. Hampson, D.R., and Blatt, G.J. (2015). Autism spectrum disorders and neuropathology of the cerebellum. Front. Neurosci. *9*, 420. https://doi.org/10.3389/fnins.2015.00420.

25. Puig, R.R., Boddie, P., Khan, A., Castro-Mondragon, J.A., and Mathelier, A. (2021). UniBind: maps of high-confidence direct TF-DNA interactions across nine species. BMC Genom. *22*, 482. https://doi.org/10.1186/s12864-021-07760-6.

26. Luo, Y., Hitz, B.C., Gabdank, I., Hilton, J.A., Kagda, M.S., Lam, B., Myers, Z., Sud, P., Jou, J., Lin, K., et al. (2020). New developments on the Encyclopedia of DNA Elements (ENCODE) data portal. Nucleic Acids Res. *48*, D882–D889. https://doi.org/10.1093/nar/gkz1062.

27. Lawler, A.J., Ramamurthy, E., Brown, A.R., Shin, N., Kim, Y., Toong, N., Kaplow, I.M., Wirthlin, M., Zhang, X., Phan, B.N., et al. (2022). Machine learning sequence prioritization for cell type-specific enhancer design. Elife *11*, e69571. https://doi.org/10.7554/eLife.69571.

28. Hollidge, B.S., Carroll, H.B., Qian, R., Fuller, M.L., Giles, A.R., Mercer, A.C., Danos, O., Liu, Y., Bruder, J.T., and Smith, J.B. (2022). Kinetics and durability of transgene expression after intrastriatal injection of AAV9 vectors. Front. Neurol. *13*, 1051559. https://doi.org/10.3389/fneur.2022.1051559.

29. Gholizadeh, S., Arsenault, J., Xuan, I.C.Y., Pacey, L.K., and Hampson, D.R. (2014). Reduced phenotypic severity following adeno-associated virus-mediated Fmr1 gene delivery in fragile X mice. Neuropsychopharmacology *39*, 3100–3111. https://doi.org/10.1038/npp.2014.167.

30. Hampson, D.R., Hooper, A.W.M., and Niibori, Y. (2019). The application of adeno-associated viral vector gene therapy to the treatment of fragile X syndrome. Brain Sci. *9*, 32. https://doi.org/10.3390/brainsci9020032.

31. Hooper, A.W.M., Wong, H., Niibori, Y., Abdoli, R., Karumuthil-Melethil, S., Qiao, C., Danos, O., Bruder, J.T., and Hampson, D.R. (2021). Gene therapy using an ortholog of human fragile X mental retardation protein partially rescues behavioral abnormalities and EEG activity. Mol. Ther. Methods Clin. Dev. *22*, 196–209. https://doi.org/10.1016/j.omtm.2021.06.013.

32. Gouwens, N.W., Sorensen, S.A., Baftizadeh, F., Budzillo, A., Lee, B.R., Jarsky, T., Alfiler, L., Baker, K., Barkan, E., Berry, K., et al. (2020). Integrated morphoelectric and transcriptomic classification of cortical GABAergic cells. Cell *183*, 935–953.e19. https://doi.org/10.1016/j.cell.2020.09.057.

33. Perez, J.D., Dieck, S.T., Alvarez-Castelao, B., Tushev, G., Chan, I.C., and Schuman, E.M. (2021). Subcellular sequencing of single neurons reveals the dendritic transcriptome of GABAergic interneurons. Elife *10*, e63092. https://doi.org/10.7554/eLife.63092.

34. Sundberg, M., and Sahin, M. (2015). Cerebellar development and autism spectrum disorder in tuberous sclerosis complex. J. Child Neurol. *30*, 1954–1962. https://doi.org/10.1177/0883073815600870.

35. Pelkey, K.A., Chittajallu, R., Craig, M.T., Tricoire, L., Wester, J.C., and McBain, C.J. (2017). Hippocampal GABAergic inhibitory interneurons. Physiol. Rev. *97*, 1619–1747. https://doi.org/10.1152/physrev.00007.2017.

36. Catania, M.V., Copani, A., Calogero, A., Ragonese, G.I., Condorelli, D.F., and Nicoletti, F. (1999). An enhanced expression of the immediate early gene, Egr-1, is associated with neuronal apoptosis in culture. Neuroscience *91*, 1529–1538. https://doi.org/10.1016/S0306-4522(98)00544-2.

37. Sánchez-Huertas, C., and Rico, B. (2011). CREB-dependent regulation of GAD65 transcription by BDNF/TrkB in cortical interneurons. Cereb. Cortex *21*, 777–788. https://doi.org/10.1093/cercor/bhq150.

38. Ghosh, I., Liu, C.S., Swardfager, W., Lanctôt, K.L., and Anderson, N.D. (2021). The potential roles of excitatory-inhibitory imbalances and the repressor element-1 silencing transcription factor in aging and aging-associated diseases. Mol. Cell. Neurosci. *117*, 103683. https://doi.org/10.1016/j.mcn.2021.103683.

39. Prestigio, C., Ferrante, D., Marte, A., Romei, A., Lignani, G., Onofri, F., Valente, P., Benfenati, F., and Baldelli, P. (2021). REST/NRSF drives homeostatic plasticity of inhibitory synapses in a target-dependent fashion. Elife *10*, e69058. https://doi.org/10.7554/eLife.69058.

40. Frazer, K.A., Pachter, L., Poliakov, A., Rubin, E.M., and Dubchak, I. (2004). VISTA: computational tools for comparative genomics. Nucleic Acids Res. *32*, W273–W279. https://doi.org/10.1093/nar/gkh458.

41. Tkatch, T., Rysevaite-Kyguoliene, K., Sabeckis, I., Sabeckiene, D., Pauza, D.H., and Baranauskas, G. (2022). An efficient rAAV vector for protein expression in cortical parvalbumin expressing interneurons. Sci. Rep. *12*, 17851. https://doi.org/10.1038/s41598-022-21867-0.